World Journal of Gastroenterology

Submit a Manuscript: https://www.f6publishing.com

*World J Gastroenterol* 2020 May 7; 26(17): 2082-2096

DOI: 10.3748/wjg.v26.i17.2082

ISSN 1007-9327 (print) ISSN 2219-2840 (online)

ORIGINAL ARTICLE

Retrospective Study

# Prediction of different stages of rectal cancer: Texture analysis based on diffusion-weighted images and apparent diffusion coefficient maps

Jian-Dong Yin, Li-Rong Song, He-Cheng Lu, Xu Zheng

**ORCID number:** Jian-Dong Yin (0000-0002-4266-6586); Li-Rong Song (0000-0002-2180-0205); He-Cheng Lu (0000-0002-8410-6894); Xu Zheng (0000-0002-2739-7111).

**Author contributions:** Yin JD designed this study; Lu HC performed the research; Song LR wrote the paper; Yin JD supervised the report; Zheng X provided clinical advice.

**Supported by** Research and Development Foundation for Major Science and Technology from Shenyang, No. 19-112-4-105; Big Data Foundation for Health Care from China Medical University, No. HMB201902105; and Natural Fund Guidance Plan from Liaoning, No. 2019-ZD-0743.

**Institutional review board statement:** This study was reviewed and approved by the Ethics Committee of Shengjing Hospital of China Medical University.

**Informed consent statement:** Written informed consent was acquired from each patient.

**Conflict-of-interest statement:** All authors declare no conflicts-of-interest related to this article.

**Data sharing statement:** No additional data are available.

**Open-Access:** This article is an open-access article that was selected by an in-house editor and fully peer-reviewed by external

**Jian-Dong Yin, Li-Rong Song,** Department of Radiology, Shengjing Hospital of China Medical University, Shenyang 110003, Liaoning Province, China

**He-Cheng Lu,** College of Medicine and Biological Information Engineering, Northeastern University, Shenyang 110036, Liaoning Province, China

**Xu Zheng,** Department of Clinical Oncology, Shengjing Hospital of China Medical University, Shenyang 110011, Liaoning Province, China

**Corresponding author:** Xu Zheng, MD, Associate Professor, Department of Clinical Oncology, Shengjing Hospital of China Medical University, No. 39, Huaxiang Street, Tiexi District, Shenyang 110011, Liaoning Province, China. cmuzhengxu@126.com

## Abstract

### *BACKGROUND*

It is evident that an accurate evaluation of T and N stage rectal cancer is essential for treatment planning. It has not been extensively investigated whether texture features derived from diffusion-weighted imaging (DWI) images and apparent diffusion coefficient (ADC) maps are associated with the extent of local invasion (pathological stage T1-2 *vs* T3-4) and nodal involvement (pathological stage N0 *vs* N1-2) in rectal cancer.

### *AIM*

To predict different stages of rectal cancer using texture analysis based on DWI images and ADC maps.

### *METHODS*

One hundred and fifteen patients with pathologically proven rectal cancer, who underwent preoperative magnetic resonance imaging, including DWI, were enrolled, retrospectively. The ADC measurements ($ADC_{mean}$, $ADC_{min}$, $ADC_{max}$) as well as texture features, including the gray level co-occurrence matrix parameters, the gray level run-length matrix parameters and wavelet parameters were calculated based on DWI ($b$ = 0 and $b$ = 1000) images and the ADC maps. Independent sample $t$-tests or Mann-Whitney $U$ tests were used for statistical analysis. Multivariate logistic regression analysis was conducted to establish the models. The predictive performance was validated by receiver operating characteristic curve analysis.

**Manuscript source**: Unsolicited Manuscript

**Received:** February 6, 2020
**Peer-review started:** February 6, 2020
**First decision:** February 29, 2020
**Revised:** March 26, 2020
**Accepted:** April 15, 2020
**Article in press:** April 15, 2020
**Published online:** May 7, 2020

**P-Reviewer:** Manenti A, Ziogas DE
**S-Editor:** Wang YQ
**L-Editor:** Webster JR
**E-Editor:** Ma YJ

*RESULTS*

Dissimilarity, sum average, information correlation and run-length nonuniformity from DWI$b_{=0}$ images, gray level nonuniformity, run percentage and run-length nonuniformity from DWI$b_{=1000}$ images, and dissimilarity and run percentage from ADC maps were found to be independent predictors of local invasion (stage T3-4). The area under the operating characteristic curve of the model reached 0.793 with a sensitivity of 78.57% and a specificity of 74.19%. Sum average, gray level nonuniformity and the horizontal components of symlet transform (SymletH) from DWI$b_{=0}$ images, sum average, information correlation, long run low gray level emphasis and SymletH from DWI$b_{=1000}$ images, and $ADC_{max}$, $ADC_{mean}$ and information correlation from ADC maps were identified as independent predictors of nodal involvement. The area under the operating characteristic curve of the model reached 0.802 with a sensitivity of 80.77% and a specificity of 68.25%.

*CONCLUSION*

Texture features extracted from DWI images and ADC maps are useful clues for predicting pathological T and N stages in rectal cancer.

**Key words:** Rectal cancer; Diffusion weighted imaging; Apparent diffusion coefficient; Texture analysis



**Core tip:** This retrospective study investigated the correlations between stages of rectal cancer and texture features from diffusion-weighted images and apparent diffusion coefficient maps. The area under the operating characteristic curve reached 0.793 for identifying local invasion (T stage), and reached 0.802 for determining nodal involvement (N stage). Texture analysis based on diffusion-weighted images and apparent diffusion coefficient maps showed potential value in classifying N and T stage rectal cancer.

**Citation:** Yin JD, Song LR, Lu HC, Zheng X. Prediction of different stages of rectal cancer: Texture analysis based on diffusion-weighted images and apparent diffusion coefficient maps. *World J Gastroenterol* 2020; 26(17): 2082-2096
**URL**: https://www.wjgnet.com/1007-9327/full/v26/i17/2082.htm
**DOI**: https://dx.doi.org/10.3748/wjg.v26.i17.2082

## INTRODUCTION

Colorectal cancer is the third leading cause of cancer worldwide, and rectal cancer accounts for approximately 30%-35% of colorectal cancer cases[1,2]. Advances in surgical techniques, chemotherapy and radiation therapy regimens have led to decreased local recurrence rates and mortality[3,4]. Available treatment options vary by tumor stage. The extent of tumor invasion into the bowel wall (pathological T stage) and the number of lymph nodes affected by the lesions (pathological N stage) are important prognostic factors for local recurrence and overall survival[5]. Rectal cancer guidelines from the National Comprehensive Cancer Network recommend neoadjuvant chemoradiotherapy (NAT) for patients with lymph node involvement before surgery[6]. Compared with surgery alone, the use of NAT followed by surgical resection for locally advanced rectal carcinoma (stage T3-4 and/or N1-2) has been shown to be associated with a 50%-61% reduction in the risk of local recurrence[7,8]. Hence, an accurate evaluation of T and N stage is essential for treatment planning.

High-resolution magnetic resonance imaging (MRI) has been widely recommended for local staging of primary rectal cancer before treatment, but has some limitations[9]. It is difficult to distinguish T2 from the T3 stage of tumors as the peritumoral inflammatory reaction is similar to tumor penetration through the muscular rectal wall[10]. In addition, the detection of tissue edema, fibrosis and inflammation can be less accurate after NAT[11]. Also, preoperative detection of nodal involvement with morphological criteria such as short-axis diameter, shape, border smoothness and signal heterogeneity is another challenge[12,13]. Thus, improved techniques for T and N

staging are of great importance.

Diffusion-weighted imaging (DWI) is a functional MRI technique for detecting the movement of water molecules in the extracellular space, which could reflect the varying cellularity of a tumor. Previous studies have indicated that the apparent diffusion coefficient (ADC) calculated from DWI could be a valuable imaging biomarker of tumor property[14]. Earlier research findings also suggested that ADC values were helpful in the detection of rectal cancers as well as the prediction of pathological complete response after NAT[15,16]. However, the ADC calculation only described the average, maximum, or minimum signal intensity within the tumors, failing to reflect their heterogeneity. Due to the intrinsic chaotic environment of the tumor, ADC values are not sufficiently sensitive to small changes or the precise status of tumors[17].

Texture analysis, which has emerged as one of the "radiomics" approaches for interpretation of medical imaging, is a tool for extracting quantitative features by measuring the spatial variation of gray levels on a pixel-by-pixel basis within given images[18]. It provides a more objective method to characterize tissue heterogeneity within the lesion that is closely correlated with tumor grading and staging. Some textures extracted from MRI or computed tomography (CT) have shown potential in several aspects, such as distinguishing benign from malignant lesions, staging preoperative cancer (N or T stage), predicting gene expression type and forecasting the result of tumor treatment[19-21]. It has been suggested that skewness and kurtosis differ significantly in cervical cancer between positive *vs* negative pelvic lymph node metastatic status[22]. In addition, contrast and difference in variance showed higher values for nonresponders than partial responders to chemotherapy[23]. It has also been shown that lower entropy, higher uniformity and lower standard deviation were associated with poorer 5-year overall survival in patients with colorectal cancer[24]. Moreover, one previous study demonstrated that higher heterogeneity of the tumor was a powerful predictor of pathologic regional lymph node metastasis in esophageal cancer[25].

The heterogeneity within the tumor originating from intratumoral spatial variation in the cellularity, angiogenesis, extravascular extracellular matrix, and necrosis could be captured by DWI images and ADC maps with texture analysis. Therefore, the aim of this study was to investigate whether texture features derived from DWI images and ADC maps were associated with the pathological stage T1-2 *vs* T3-4 and pathological stage N0 *vs* N1-2 in rectal cancer. To our best knowledge, texture analysis of DWI images combined with ADC maps for preoperative staging of rectal cancer has not been documented.

## MATERIALS AND METHODS

The study was approved by the Ethics Review Board of Shengjing Hospital of China Medical University (2020PS011K), and written informed consent was obtained from each patient.

### Patients

All cases ($n$ = 362) with rectal MRIs were browsed using the Picture Archiving and Communication System in our institution between September 2018 and November 2019. Inclusion criteria were as follows: (1) Patients with preoperative DWI; (2) Patients who underwent radical resection within 1 month after high-resolution MRI scanning; (3) Patients with rectal adenocarcinoma confirmed by surgical specimen; and (4) Patients with only one lesion identified for subsequent analysis. Initially, the population comprised 168 rectal cancer patients. Fifty-three patients were excluded for the following reasons: (1) Patients underwent NAT or endoscopic biopsy before MRI scanning; (2) Image quality was poor due to apparent motion artifacts on the DWI sequence; (3) Pathological data were incomplete (such as lack of N- or T-staging information); and (4) Patients had pathologically proven mucinous adenocarcinoma which tended to have a low cellular density resulting in high ADC values that might bias results. Finally, 115 eligible patients were selected for subsequent analyses. The clinical characteristics of these patients are shown in Table 1. The flowchart of this study is displayed in Figure 1.

### MRI techniques

All MRI examinations were performed on a 3.0-Tesla (T) scanner (Ingenia 3.0, Philips Medical System, Best, The Netherlands) with an eight-channel phased-array surface coil in the supine position. There was no bowel preparation or intravenous antispasmodic agents administered. An axial DWI sequence was performed for all patients. The acquisition parameters were as follows: Repetition time/echo time,

**Table 1 Clinical and pathological characteristics of the patients**

| Characteristics | Value |
|---|---|
| Total patients | 115 |
| Age, yr | 60.4 ± 15.8 (32-86)[1] |
| Gender | |
| Male | 67 (58.3) |
| Female | 48 (41.7) |
| Primary mass location (from anal verge) | |
| 0-5 cm | 35 (30.5) |
| 5.1-10 cm | 58 (50.4) |
| 10.1-15 cm | 22 (19.1) |
| Tumor differentiation | |
| Moderate to high | 89 (77.4) |
| Low | 26 (22.6) |
| T stage | |
| T1-2 | 31 (26.9) |
| T3-4 | 84 (73.1) |
| N stage | |
| N0 | 63 (54.7) |
| N1-2 | 52 (45.3) |

[1]mean ± SD (range in years). Unless otherwise indicated, variables are expressed as frequencies (%).

6000/76 ms; flip angle, 90°; matrix size, 288 × 288; field of view, 450 mm; slices, 48; slice thickness, 5 mm; spacing between slices, 1 mm; *b* values, 0 and 1000 s/mm$^2$.

### Lesion segment

ADC maps were generated with MATLAB 2018a (Mathworks, Natick, MA, United States) according to loaded DWI images using the following formula: ADC = (ln$SI_0$-lnSI)/(*b*-*b0*) where $SI_0$ and SI represent signal intensity at *b* values of 0 and 1000 s/mm$^2$, respectively.

Region of interest (ROI) segmentation was performed independently by two radiologists with 10 years of experience in interpreting pelvic MRIs who were blinded to the pathological results. The ADC maps were imported into image processing software (ImageJ, National Institutes of Health, Bethesda, MD, United States) for segmentation of ROIs. Rectal cancer was determined as a local mass or abnormal wall thickening that showed intermediate intensity of signals on T2WI, hyperintensity on DWI and hypointensity on the ADC map. ROIs were manually delineated along the border of the low signal area on the single slice of the ADC map, which showed the largest tumor diameter with reference to T2WI and DWI. Obvious necrosis, gas and lumen content areas were avoided to minimize bias. The contours of ROIs on ADC maps were copied to the exact same location of the corresponding DWI images (*b* = 0 and *b* = 1000).

### Texture analysis

Texture parameters were extracted from ADC maps, DWI$b_{=0}$ images and DWI$b_{=1000}$ images using in-house software programmed with MATLAB 2018a. Twelve texture features were calculated based on three images for each patient from the gray level co-occurrence matrix, the gray level run-length matrix and wavelet. The mean ADC values, minimum and maximum ADC values ($ADC_{mean}$, $ADC_{min}$, $ADC_{max}$) were also calculated. Therefore, a total of 39 features were measured for each patient. A detailed description of these features is provided in Table 2.

### Statistical analysis

A Kolmogorov-Smirnov test for each feature was first performed to confirm that the samples followed a normal distribution. If the distribution was normal ($P \geq 0.05$), an independent sample *t*-test was used to compare parameters between T1-2 and T3-4 stages, and between N0 and N1-2 stages. Otherwise, the Mann-Whitney *U* test was used[26]. Those significantly different parameters were selected for subsequent analysis. Multivariate logistic regression analysis was performed with the entry of variables to identify independent factors for T3-4 and N1-2 tumors. In addition,

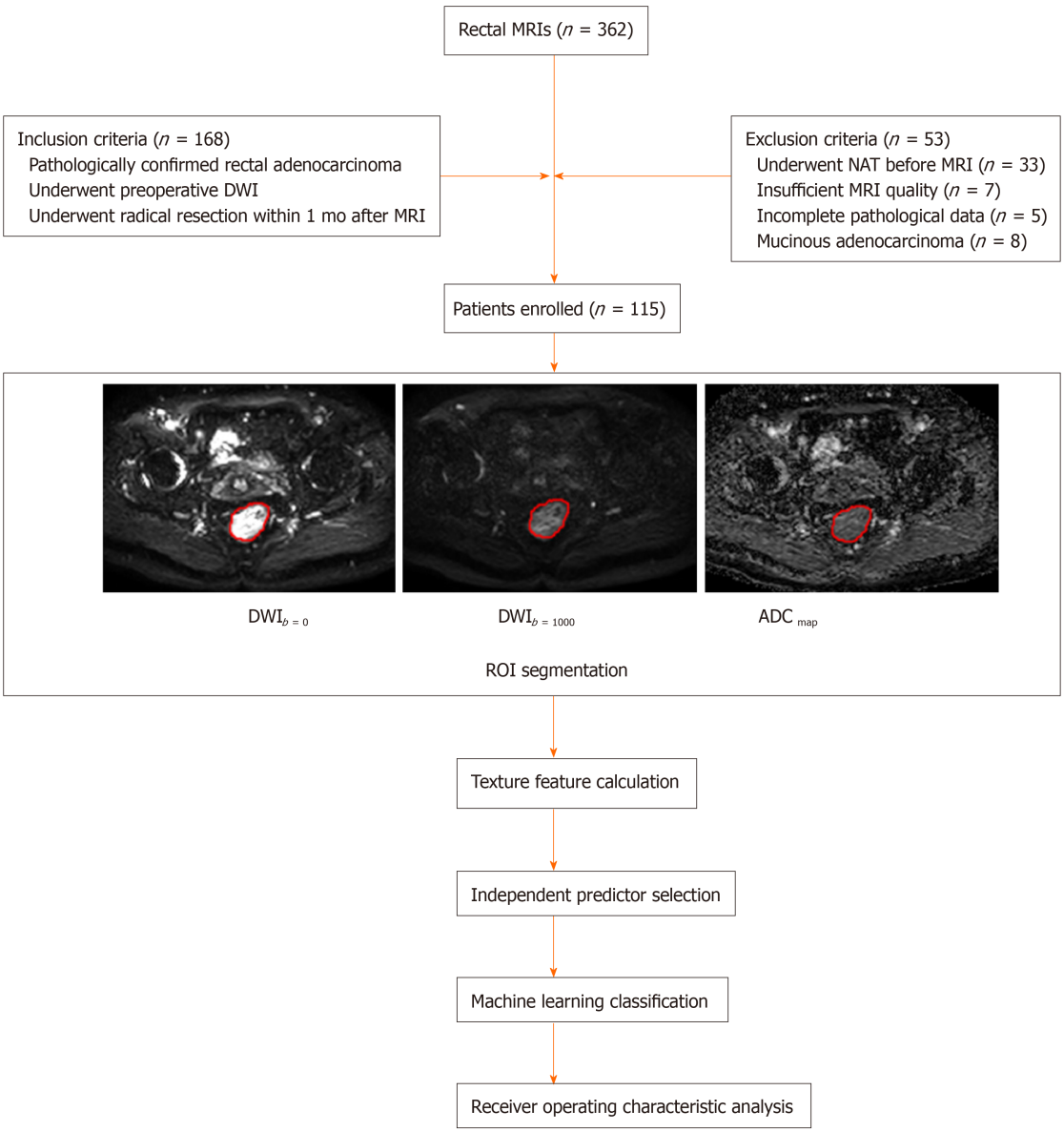


**Figure 1 Flow chart adopted in this study.** MRI: Magnetic resonance imaging; DWI: Diffusion-weighted imaging; NAT: Neoadjuvant chemoradiotherapy; ADC: Apparent diffusion coefficient; ROI: Region of interest.

Spearman correlation analysis was performed to assess the correlation between features and tumor stages. Receiver operating characteristic (ROC) curve analysis was conducted to evaluate the diagnostic performance of the established logistic models for prediction of T3-4 and N1-2 tumors by calculating the area under the ROC curve (AUC), which was drawn with the professional statistics software MedCalc (version 14.10.20, http://www.medcalc.org/). The corresponding sensitivity and specificity were also calculated. Interobserver variability of texture features extracted between the two radiologists was evaluated using intraclass correlation coefficients (0-0.4, poor agreement; 0.41-0.6, moderate agreement; 0.61-0.8, good agreement; 0.81-1, excellent agreement). All statistical analyses were performed using SPSS 22.0 (IBM, Armonk, NY, United States). $P < 0.05$ was considered statistically significant.

## RESULTS

A randomly selected case was used to illustrate the ROI segmentation results, as shown in Figure 2. The results of texture analysis for identifying T- and N- stage are described as follows:

**Table 2 Features measured by different methods**

| Analysis method | Feature |
|---|---|
| ADC | $ADC_{min}$ |
| | $ADC_{max}$ |
| | $ADC_{mean}$ |
| Gray level co-occurrence matrix | Dissimilarity |
| | Sum average |
| | Difference variance |
| | Information correlation |
| Gray level run-length matrix | Gray level nonuniformity |
| | Run percentage |
| | Long run low gray level emphasis |
| | Run-length nonuniformity |
| Wavelet | SymletL |
| | SymletH |
| | SymletV |
| | SymletD |

ADC: Apparent diffusion coefficient.

### *Features between stage T1-2 and T3-4 tumors*

All significantly different texture features between stage T1-2 *vs* T3-4 groups are summarized in Table 3. No significant difference was observed with respect to any of the ADC measurements. The logistic regression model that incorporated features from DWI$b_{=0}$ images that were significantly different between stage T1-2 and T3-4 tumors reached an AUC of 0.710 (sensitivity, 65.48%; specificity, 72.86%; accuracy, 70.87%; 95% confidence interval (CI): 0.618-0.791). The logistic regression model that incorporated significantly different features from DWI$b_{=1000}$ images achieved an AUC of 0.688 (sensitivity, 61.90%; specificity, 70.97%; accuracy, 68.52%; 95%CI: 0.595-0.771). In addition, the logistic regression model that incorporated significantly different features from ADC maps achieved an AUC of 0.657 (sensitivity, 45.24%; specificity, 83.87%; accuracy, 73.46; 95%CI: 0.563-0.743). The above significantly different features were used as input variables for the multivariate logistic regression analysis. For DWI$b_{=0}$ features, higher dissimilarity, higher sum average, higher information correlation and lower run-length nonuniformity were found to be independent predictors of local invasion (stage T3-4). For DWI$b_{=1000}$ features, higher gray level nonuniformity, higher run percentage and lower run-length nonuniformity were found to be independent predictors. For ADC map features, lower dissimilarity and higher run percentage were determined to be independent predictors. Using the logistic regression model that incorporated these nine features for differentiating stage T3-4 from T1-2 tumors, an AUC of 0.793 was achieved with a sensitivity of 78.57% and a specificity of 74.19%, and the accuracy was 75.37% with 95%CI of 0.707-0.863. The ROC curves are shown in Figure 3. The Spearman correlation coefficients of the predictors for T stage are listed in Table 4. Among these features, run-length nonuniformity from DWI$b_{=1000}$ images showed the highest correlation with T stage ($R_s$ = 0.246, $P$ = 0.008).

### *Features between stage N0 and N1-2 tumors*

The significantly different texture features and ADC values between stage N0 and N1-2 tumors are summarized in Table 5. With regard to the features from ADC maps, $ADC_{max}$ and $ADC_{mean}$ showed statistically significant differences between the groups ($P$ = 0.011, and 0.001, respectively). The logistic regression model that incorporated statistically significant features extracted from DWI$b_{=0}$ images achieved an AUC of 0.623 (sensitivity, 79.65%; specificity, 42.86%; accuracy, 63.01%; 95%CI: 0.528-0.711). Using the logistic regression model that incorporated significantly different features derived from DWI$b_{=1000}$ images, the AUC reached 0.635 (sensitivity, 57.69%; specificity, 66.67%; accuracy, 61.75%; 95%CI: 0.540-0.723). Using the logistic regression model that incorporated significantly different features obtained from ADC maps, the AUC was 0.714 (sensitivity, 75.02%; specificity, 65.08%; accuracy, 70.52%; 95%CI: 0.622-0.794). In addition, multivariate logistic regression analysis showed that lower sum average, lower gray level nonuniformity and higher SymletH from DWI$b_{=0}$ images were

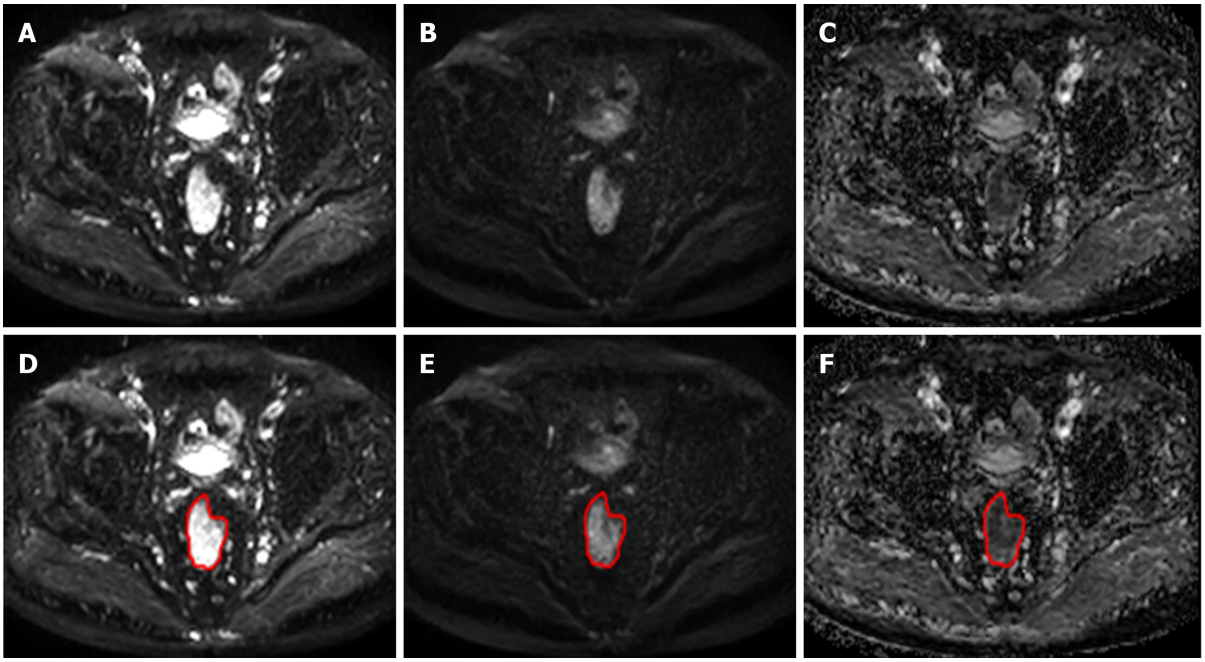


**Figure 2 The region of interest segmentation results for a randomly selected case.** A-C: Represent diffusion-weighted imaging (DWI)$b_{=0}$, DWI$b_{=1000}$ and the apparent diffusion coefficient image on the same slice, respectively; D-F: With regard to T2WI and DWI, the lesion region of interest was drawn on the apparent diffusion coefficient map (F) and copied onto the DWI$b_{=0}$ (D) and DWI$b_{=1000}$ (E) images.

independent predictors of nodal involvement (N1-2); from DWI$b_{=1000}$ images, lower sum average, lower information correlation, lower long run low gray level emphasis and higher SymletH were independent predictors; and for ADC maps, the independent predictors were lower $ADC_{max}$, lower $ADC_{mean}$ and lower information correlation. The logistic regression model that incorporated these ten features for distinguishing stage N0 and N1-2 tumors achieved an AUC of 0.802 with a sensitivity of 80.77% and a specificity of 68.25%, and the accuracy was 75.11% with 95%CI of 0.718-0.871. The Spearman correlation coefficients for the predictors of N stage are shown in Table 6. Of these features, $ADC_{mean}$ showed the strongest correlation with N stage ($R_s$ = -0.273, $P$ = 0.003). The ROC curves are shown in Figure 4.

### *Interobserver agreement evaluation*

There was excellent agreement between the ADC measurements and texture features derived from the two sets of ROIs independently delineated by two radiologists based on $DWI_{b0/b1000}$ images and ADC maps. The intraclass correlation coefficients ranged from 0.844 to 0.960.

## DISCUSSION

In the present study, texture analysis was performed based on DWI images and ADC maps, and the correlation between texture features and T/N stage of rectal cancer was investigated. The results demonstrated the potential of texture features for staging rectal cancer.

Extramural invasion and nodal involvement are the main indications for the use of NAT in patients with rectal cancer[8]. Currently, the accuracy of preoperative staging by rectal MRI is still unsatisfactory[27,28]. Therefore, improved techniques for T and N staging may play an important role in determining the best treatment options for patients. Texture analysis provides a method for quantifying the intratumoral heterogeneity based on the distribution of gray level values and spatial arrangement of the pixels. In particular, texture analysis has been acknowledged as a promising tool for distinguishing benign from malignant tumors and in the staging of kidney and cervical cancer[29,30]. However, few studies on rectal MRI using texture analysis have been conducted to identify noninvasive independent predictors of high T stage and positive nodal status[31]. Furthermore, the independent predictors identified in these studies were derived from conventional morphological images, while our study mainly concentrated on functional DWI images ($b$ = 0/ $b$ = 1000) and ADC maps.

In this study, eight texture features (run-length nonuniformity, information

**Table 3 Comparison of extracted features between T1-2 and T3-4 stage groups of rectal cancers**

| Method | Features | T1-2 (*n* = 31) | T3-4 (*n* = 84) | *P* value |
|---|---|---|---|---|
| DWI$b_{=0}$ | Dissimilarity | 0.015 ± 0.008 | 0.018 ± 0.013 | 0.017[2] |
| | Sum average | 2.068 ± 0.043 | 2.095 ± 0.067 | 0.018[1] |
| | Difference variance | 0.140 ± 0.085 | 0.161 ± 0.192 | 0.135[2] |
| | Information correlation | 0.185 ± 0.058 | 0.215 ± 0.067 | 0.016[2] |
| | Gray level nonuniformity | 1.411 ± 0.351 | 1.730 ± 0.811 | 0.019[1] |
| | Run percentage | 0.075 ± 0.012 | 0.083 ± 0.023 | 0.009[2] |
| | Long run low gray level emphasis | 4.971 ± 4.897 | 5.840 ± 4.678 | 0.316[2] |
| | Run-length nonuniformity | 3.266 ± 0.356 | 3.107 ± 0.445 | 0.030[1] |
| | SymletL | 7.815 ± 1.568 | 8.295 ± 1.153 | 0.367[2] |
| | SymletH | 0.627 ± 0.4011 | 0.516 ± 0.318 | 0.221[1] |
| | SymletV | 0.335 ± 0.460 | 0.359 ± 0.298 | 0.816[2] |
| | SymletD | 0.162 ± 0.158 | 0.177 ± 0.114 | 0.371[2] |
| DWI$b_{=1000}$ | Dissimilarity | 0.018 ± 0.006 | 0.021 ± 0.018 | 0.060[2] |
| | Sum average | 2.098 ± 0.058 | 2.122 ± 0.076 | 0.121[1] |
| | Difference variance | 0.176 ± 0.105 | 0.198 ± 0.257 | 0.348[2] |
| | Information correlation | 0.194 ± 0.041 | 0.217 ± 0.058 | 0.053[1] |
| | Gray level nonuniformity | 1.443 ± 0.370 | 1.773 ± 0.815 | 0.021[1] |
| | Run percentage | 0.075 ± 0.014 | 0.083 ± 0.023 | 0.009[2] |
| | Long run low gray level emphasis | 8.801 ± 5.347 | 8.646 ± 7.836 | 0.980[2] |
| | Run-length nonuniformity | 3.239 ± 0.371 | 3.084 ± 0.461 | 0.036[1] |
| | SymletL | 8.461 ± 1.329 | 8.749 ± 0.984 | 0.935[2] |
| | SymletH | 0.318 ± 0.387 | 0.336 ± 0.261 | 0.696[2] |
| | SymletV | 0.293 ± 0.371 | 0.316 ± 0.249 | 0.501[2] |
| | SymletD | 0.099 ± 0.124 | 0.118 ± 0.113 | 0.137[2] |
| ADC maps | $ADC_{min}$ | 0.328 ± 0.385 | 0.262 ± 0.367 | 0.745[2] |
| | $ADC_{max}$ | 2.513 ± 0.855 | 2.704 ± 0.885 | 0.298[1] |
| | $ADC_{mean}$ | 1.099 ± 0.471 | 1.063 ± 0.521 | 0.740[1] |
| | Dissimilarity | 0.062 ± 0.008 | 0.021 ± 0.011 | 0.020[2] |
| | Sum average | 2.049 ± 0.038 | 2.063 ± 0.061 | 0.171[2] |
| | Difference variance | 0.170 ± 0.122 | 0.218 ± 0.135 | 0.137[2] |
| | Information correlation | 0.181 ± 0.041 | 0.199 ± 0.052 | 0.055[1] |
| | Gray level nonuniformity | 1.367 ± 0.334 | 1.675 ± 0.739 | 0.014[1] |
| | Run percentage | 0.073 ± 0.011 | 0.082 ± 0.021 | 0.012[2] |
| | Long run low gray level emphasis | 4.006 ± 4.016 | 4.558 ± 4.364 | 0.860[2] |
| | Run-length nonuniformity | 3.309 ± 0.498 | 3.168 ± 4.328 | 0.068[1] |
| | SymletL | 6.789 ± 1.253 | 6.607 ± 1.435 | 0.525[1] |
| | SymletH | 0.443 ± 0.187 | 0.530 ± 0.261 | 0.791[1] |
| | SymletV | 0.473 ± 0.358 | 0.572 ± 0.350 | 0.199[2] |
| | SymletD | 0.313 ± 0.224 | 0.301 ± 0.166 | 0.905[1] |

[1]Independent samples *t*-test, data are means ± SD.
[2]Mann-Whitney *U* test, data are medians ± interquartile range. DWI: Diffusion-weighted imaging; ADC: Apparent diffusion coefficient.

correlation, SymletH, long run low gray level emphasis, sum average, gray level nonuniformity, dissimilarity and run percentage) presented statistically significant differences between groups and were employed for predicting T/N stage of rectal cancer. Theoretically, run-length nonuniformity means similarity of the length of runs derived from gray level run-length matrix, information correlation means nonlinear gray level dependence derived from gray level co-occurrence matrix, SymletH means horizontal components of symlet transform derived from Wavelet, long run low gray level emphasis means distribution of long runs and high gray level derived from gray level run-length matrix, sum average means over brightness derived from gray level co-occurrence matrix, gray level nonuniformity means similarity of the gray level value derived from gray level run-length matrix, dissimilarity means local contrast derived from gray level co-occurrence matrix, and run percentage means the homogeneity and the distribution derived from gray level run-length matrix, respectively.

In the present study, we found that six texture features from DWI$b_{=0}$ images, three features from DWI$b_{=1000}$ images and three features from ADC maps were significantly different between stage T1-2 and T3-4 tumors. Moreover, it was found that higher dissimilarity, higher sum average, higher information correlation and lower run-length nonuniformity from DWI$b_{=0}$ images were independent predictors of local invasion, as were higher gray level nonuniformity, higher run percentage and lower run-length nonuniformity from DWI$b_{=1000}$ images, while lower dissimilarity and higher run percentage from ADC maps were also independent predictors. The performance (AUC = 0.793) of the model that contained these independent predictors derived by logistic regression analysis was more favorable than the performance of the models that contained significant features independently extracted from the two types of DWI images and ADC maps. Furthermore, there were no significant differences between ADC measurements ($ADC_{mean}$, $ADC_{min}$ or $ADC_{max}$) for the T1-2 and T3-4 groups in our study. These findings are consistent with earlier reports by Liu *et al*[31] and Attenberger *et al*[32]. In fact, routine measurements of ADC are just conducted by calculating the intensities within a ROI, and the heterogenous intensities of different areas could offset each other. That means ADC quantification may mask some useful information about the tumor, while texture analysis can capture the spatial distribution of intensities, which rendered it as a more informative analysis method and a complement to routine ADC measurements. On the other hand, the lack of statistical significance might be because of the relatively small patient population.

Nodal involvement may be an indication for preoperative NAT in rectal cancer. Numerous previous studies have used size as the criterion for evaluating nodal metastases, but the size cutoff values for distinguishing benign from malignant nodes are inconsistent. In the present study, we found that three texture features from DWI$b_{=0}$ images, four texture features from DWI$b_{=1000}$ images and one texture feature from ADC maps were significantly different between stage N0 and N1-2 groups. In addition, ADC values ($ADC_{max}$ and $ADC_{mean}$) were also significant parameters with discrimination value. This is consistent with a recent study by Vignati *et al*[33], in which the correlation between ADC texture features and grading of prostate cancer was investigated. However, our findings were in conflict with the study by Li *et al*[34], which concluded that none of the ADCs showed any significant difference in predicting N stage. Such contradiction might be induced by the way tumors were identified. In our study, the lesions were extracted on a single ADC slice with the largest tumor diameter, while in the study by Li *et al*[34], the features were derived from the whole-lesion volume. Our experimental results also proved that lower sum average, lower gray level nonuniformity and higher SymletH from DWI$b_{=0}$ images, lower sum average, lower information correlation, lower long run low gray level emphasis and higher SymletH from DWI$b_{=1000}$ images, and lower $ADC_{max}$, lower $ADC_{mean}$ and lower information correlation from ADC maps appeared to be independent predictors of nodal involvement. By using the logistic regression model that factored these independent predictors, the performance (AUC = 0.802) for predicting N stage was better than that obtained from three other models that included significant features derived from the two types of DWI images and ADC maps, respectively. Therefore, it may be valuable to predict nodal status using the texture features based on medical images of rectal cancer. Huang *et al*[35] reported the performance of texture analysis in determining N stage based on CT images. Their

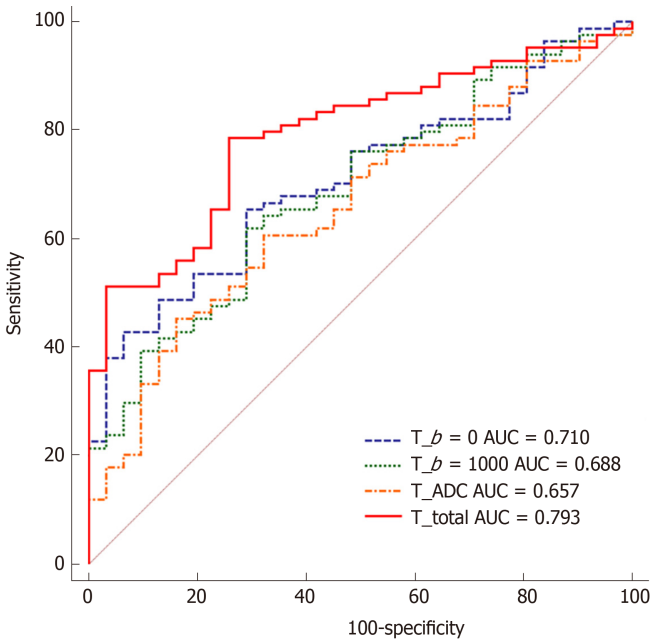


**Figure 3 Receiver operating characteristic curves obtained with different discriminatory models for predicting T1-2 and T3-4 stage tumors.** AUC: Area under the receiver operating characteristic curve; ADC: Apparent diffusion coefficient.

proposed method showed slightly lower efficiency (AUC = 0.736) than our method (AUC = 0.802). As pointed out by Lubner *et al*[36], CT acquisition parameters that influence attenuation or pixel relationships may affect texture measures. In addition to the absence of ionizing radiation, MRI is capable of multiparametric imaging, and can provide not only morphological but also functional images. MRI signal intensity is related to many factors, such as strength and uniformity of the main magnetic field, the sequence used, and the imaging parameters used (repetition time/echo time, trigger angle, and others). Thus, the application of MRI has been thought to be complicated by many issues, which brings high soft-tissue contrast and non-invasive assessment of the microcirculation of tumor. Previous studies demonstrated that in comparison with CT, MRI can provide more valuable data for radiomics through high-throughput extraction of quantitative image features. Thus, relative to CT, MRI undoubtedly has greater advantages in reflecting tumor heterogeneity and primary tumor stage for rectal cancer diagnosis, and is strongly recommended by the American Society of Colon and Rectal Surgeons to be performed before treatment[37].

In addition, interobserver variability for the calculation of ADC values and texture features based on the single-slice method between two radiologists was also evaluated. The results indicated excellent agreement with intraclass correlation coefficients ranging from 0.844 to 0.960. The variability mainly originated from slice selection and ROI delineation. Thus, it will be important to standardize strategies for ROI definition.

There are some limitations in this study. Firstly, it was a retrospective study with a relatively small sample size which impedes the generalizability of the findings. Secondly, texture analysis was performed based on a single-slice image which showed the largest diameter of the tumor, rather than the whole tumor volume. As rectal cancer usually grows along the rectal wall and forms an irregular shape, ROI delineation with a single-slice method may not accurately represent the actual shape. Thirdly, the findings may not apply to advanced rectal cancer as we only enrolled patients who underwent surgical resection directly rather than those who first received NAT. Finally, the calculated features are sensitive to the applied *b*-values. We only analyzed DWI of $b = 0$ and $b = 1000$ images and the corresponding ADC maps. More choice in *b*-values should be considered in the future.

In conclusion, texture features extracted from DWI images and ADC maps are useful clues for predicting pathological T and N stages in rectal cancer. This method may help radiologists perform accurate staging and therefore help improve individualized treatment planning.

**Table 4 Spearman correlation coefficients for independent predictors of T-stage**

| Features | T stage | |
|---|---|---|
| | $R_s$ | *P* value |
| DWI$b_{=0}$ | | |
| Dissimilarity | 0.224 | 0.016 |
| Sum average | 0.221 | 0.018 |
| Information correlation | 0.227 | 0.015 |
| Run-length nonuniformity | -0.204 | 0.029 |
| DWI$b_{=1000}$ | | |
| Gray level nonuniformity | 0.217 | 0.021 |
| Run percentage | -0.197 | 0.035 |
| Run-length nonuniformity | 0.246 | 0.008 |
| ADC map | | |
| Dissimilarity | 0.218 | 0.019 |
| Run percentage | 0.236 | 0.011 |

DWI: Diffusion-weighted imaging; ADC: Apparent diffusion coefficient.

**Table 5 Comparison of extracted features between N0 and N1-2 stage groups of rectal cancers**

| Method | Features | N0 (*n* = 63) | N1-2 (*n* = 52) | *P* value |
|---|---|---|---|---|
| DWI$b_{=0}$ | Dissimilarity | 0.018 ± 0.015 | 0.017 ± 0.011 | 0.218[2] |
| | Sum average | 2.099 ± 0.067 | 2.075 ± 0.053 | 0.045[1] |
| | Difference variance | 0.151 ± 0.145 | 0.146 ± 0.181 | 0.334[2] |
| | Information correlation | 0.211 ± 0.076 | 0.206 ± 0.063 | 0.052[2] |
| | Gray level nonuniformity | 1.727 ± 0.623 | 1.559 ± 0.884 | 0.039[1] |
| | Run percentage | 0.079 ± 0.022 | 0.078 ± 0.021 | 0.071[2] |
| | Long run low gray level emphasis | 5.943 ± 5.191 | 5.527 ± 4.137 | 0.122[2] |
| | Run-length nonuniformity | 3.082 ± 0.425 | 3.232 ± 0.493 | 0.064[1] |
| | SymletL | 8.301 ± 1.159 | 7.945 ± 1.279 | 0.058[2] |
| | SymletH | 0.487 ± 0.332 | 0.618 ± 0.349 | 0.025[1] |
| | SymletV | 0.348 ± 0.351 | 0.378 ± 0.346 | 0.702[2] |
| | SymletD | 0.158 ± 0.124 | 0.181 ± 0.449 | 0.144[2] |
| DWI$b_{=000}$ | Dissimilarity | 0.021 ± 0.022 | 0.019 ± 0.012 | 0.118[2] |
| | Sum average | 2.131 ± 0.075 | 2.098 ± 0.066 | 0.026[1] |
| | Difference variance | 0.194 ± 0.203 | 0.192 ± 0.183 | 0.291[2] |
| | Information correlation | 0.221 ± 0.053 | 0.198 ± 0.057 | 0.035[1] |
| | Gray level nonuniformity | 1.759 ± 0.639 | 1.693 ± 0.836 | 0.053[1] |
| | Run percentage | 0.081 ± 0.023 | 0.078 ± 0.022 | 0.067[2] |
| | Long run low gray level emphasis | 9.539 ± 7.4371 | 7.835 ± 5.752 | 0.017[2] |
| | Run-length nonuniformity | 3.562 ± 0.4327 | 3.210 ± 0.442 | 0.070[1] |
| | SymletL | 8.837 ± 1.013 | 8.501 ± 1.264 | 0.055[2] |
| | SymletH | 0.260 ± 0.316 | 0.374 ± 0.339 | 0.033[2] |
| | SymletV | 0.314 ± 0.339 | 0.327 ± 0.248 | 0.337[2] |
| | SymletD | 0.101 ± 0.104 | 0.125 ± 0.157 | 0.236[2] |
| ADC maps | $ADC_{min}$ | 0.645 ± 0.347 | 0.606 ± 0.539 | 0.772[2] |
| | $ADC_{max}$ | 2.642 ± 0.859 | 2.423 ± 0.857 | 0.011[1] |
| | $ADC_{mean}$ | 1.208 ± 0.515 | 0.910 ± 0.446 | 0.001[1] |
| | Dissimilarity | 0.021 ± 0.012 | 0.018 ± 0.010 | 0.435[2] |

| | | | | |
|---|---|---|---|---|
| | Sum average | 2.065 ± 0.062 | 2.049 ± 0.046 | 0.185[2] |
| | Difference variance | 0.199 ± 0.161 | 0.218 ± 0.153 | 0.813[2] |
| | Information correlation | 0.204 ± 0.483 | 0.182 ± 0.492 | 0.021[1] |
| | Gray level nonuniformity | 1.665 ± 0.628 | 1.545 ± 0.709 | 0.072[1] |
| | Run percentage | 0.079 ± 0.023 | 0.076 ± 0.021 | 0.069[2] |
| | Long run low gray level emphasis | 4.470 ± 4.194 | 4.377 ± 4.385 | 0.578[2] |
| | Run-length nonuniformity | 3.185 ± 0.387 | 3.317 ± 0.367 | 0.106[1] |
| | SymletL | 6.902 ± 1.184 | 6.358 ± 1.555 | 0.041[1] |
| | SymletH | 0.502 ± 0.247 | 0.511 ± 0.245 | 0.960[1] |
| | SymletV | 0.510 ± 0.337 | 0.578 ± 0.338 | 0.387[2] |
| | SymletD | 0.270 ± 0.133 | 0.343 ± 0.224 | 0.142[1] |

[1]Independent samples *t*-test, data are means ± SD.
[2]Mann-Whitney *U* test, data are medians ± interquartile range. DWI: Diffusion-weighted imaging; ADC: Apparent diffusion coefficient.

**Table 6 Spearman correlation coefficients for independent predictors of N-stage**

| Features | N stage | |
|---|---|---|
| | $R_s$ | *P* value |
| DWI$b_{=0}$ | | |
| Sum average | -0.188 | 0.044 |
| Gray level nonuniformity | -0.149 | 0.038 |
| SymletH | 0.211 | 0.024 |
| DWI$b_{=1000}$ | | |
| Sum average | -0.209 | 0.025 |
| Information correlation | -0.187 | 0.045 |
| Long run low gray level emphasis | -0.223 | 0.017 |
| SymletH | 0.199 | 0.033 |
| ADC maps | | |
| $ADC_{max}$ | -0.204 | 0.029 |
| $ADC_{mean}$ | -0.273 | 0.003 |
| Information correlation | -0.199 | 0.033 |

DWI: Diffusion-weighted imaging; ADC: Apparent diffusion coefficient.

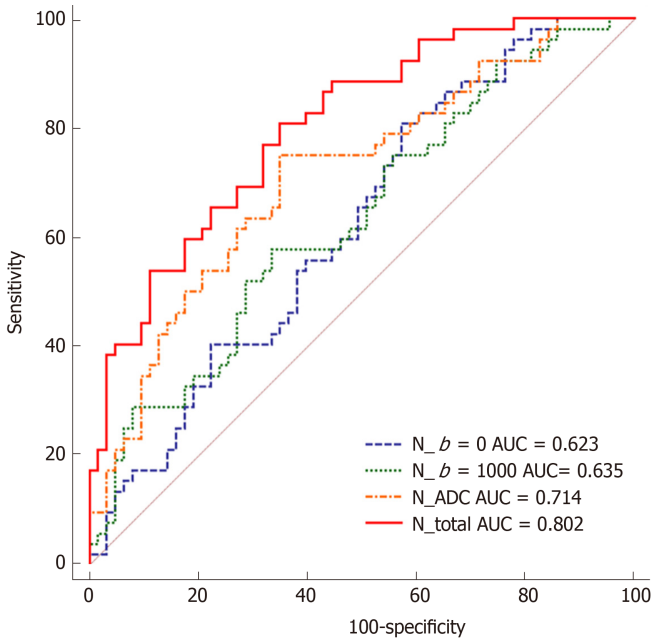


**Figure 4 Receiver operating characteristic curves obtained with different discriminatory models for predicting N0 and N1-2 stage tumors.** AUC: Area under the receiver operating characteristic curve; ADC: Apparent diffusion coefficient.

## ARTICLE HIGHLIGHTS

### *Research background*

Colorectal cancer is the third leading cause of cancer worldwide, and rectal cancer accounts for approximately 30%-35% of colorectal cancer cases. An accurate evaluation of T and N stage in rectal cancer is essential for treatment planning. Heterogeneity within the tumor is a powerful predictor of pathological stage, which can be captured by diffusion-weighted imaging (DWI) images and apparent diffusion coefficient (ADC) maps with texture analysis.

### *Research motivation*

A search of PubMed database indicates that texture analysis of DWI images combined with ADC maps for preoperative staging of rectal cancer has not been reported.

### *Research objectives*

The aim of this study was to investigate whether texture features derived from DWI images and ADC maps were associated with the pathological stage T1-2 *vs* T3-4 and pathological stage N0 *vs* N1-2 in rectal cancer.

### *Research methods*

One hundred and fifteen eligible patients were selected for analyses. Lesion segmentation was performed manually. Twelve texture features were calculated from DWI images and ADC maps, including the gray level co-occurrence matrix parameters, the gray level run-length matrix parameters and wavelet parameters. Moreover, ADC values were measured from the lesion area. An independent sample *t*-test or Mann-Whitney *U* test was used to compare parameters between T1-2 and T3-4 stages, and between N0 and N1-2 stages. Multivariate logistic regression analysis was performed with the entry of variables to identify independent factors for T3-4 and N1-2 tumors. Receiver operating characteristic analysis was conducted to evaluate the diagnostic performance of the established logistic models for prediction of T3-4 and N1-2 tumors by calculating the area under the receiver operating curve (AUC).

### *Research results*

Dissimilarity, sum average, information correlation and run-length nonuniformity from DWI$b_{=0}$ images, gray level nonuniformity, run percentage and run-length nonuniformity from DWI$b_{=1000}$ images, and dissimilarity and run percentage from ADC maps were found to be independent predictors of local invasion (stage T3-4). The AUC of the model reached 0.793 with a sensitivity of 78.57% and a specificity of 74.19%. Sum average, gray level nonuniformity and the horizontal components of symlet transform from DWI$b_{=0}$ images, sum average, information correlation, long run low gray level emphasis and horizontal components of symlet transform from DWI$b_{=1000}$ images, and $ADC_{max}$, $ADC_{mean}$ and information correlation from ADC maps were identified as independent predictors of nodal involvement. The AUC of the model reached 0.802 with a sensitivity of 80.77% and a specificity of 68.25%.

### *Research conclusions*

The results indicated that texture features derived from preoperative DWI images combined with ADC maps were significantly associated with T and N stage in rectal cancer. These findings may be of value for the selection of treatment strategies.

### *Research perspectives*

In this project, we evaluated the role of ADC maps and DWI images in determining pathological stage, and the results revealed that texture features could be considered as novel biomarkers to predict the N and T stage in rectal cancer. In a subsequent study, a randomized multi-center prospective trial could be conducted to further validate our findings.

## ACKNOWLEDGEMENTS

We thank the Shengjing Hospital of China Medical University for providing data and support.

## REFERENCES

1 **Siegel RL**, Miller KD, Jemal A. Cancer statistics, 2020. *CA Cancer J Clin* 2020; **70**: 7-30 [PMID: 31912902 DOI: 10.3322/caac.21590]
2 **Glynne-Jones R**, Wyrwicz L, Tiret E, Brown G, Rödel C, Cervantes A, Arnold D; ESMO Guidelines Committee. Rectal cancer: ESMO Clinical Practice Guidelines for diagnosis, treatment and follow-up. *Ann Oncol* 2018; **29**: iv263 [PMID: 29741565 DOI: 10.1093/annonc/mdy161]
3 **Heald RJ**, Ryall RD. Recurrence and survival after total mesorectal excision for rectal cancer. *Lancet* 1986; **1**: 1479-1482 [PMID: 2425199 DOI: 10.1016/s0140-6736(86)91510-2]
4 **Aitken RJ**. Mesorectal excision for rectal cancer. *Br J Surg* 1996; **83**: 214-216 [PMID: 8689166 DOI: 10.1046/j.1365-2168.1996.02057.x]
5 **Valentini V**, van Stiphout RG, Lammering G, Gambacorta MA, Barba MC, Bebenek M, Bonnetain F, Bosset JF, Bujko K, Cionini L, Gerard JP, Rödel C, Sainato A, Sauer R, Minsky BD, Collette L, Lambin P. Nomograms for predicting local recurrence, distant metastases, and overall survival for patients with locally advanced rectal cancer on the basis of European randomized clinical trials. *J Clin Oncol* 2011; **29**: 3163-3172 [PMID: 21747092 DOI: 10.1200/JCO.2010.33.1595]
6 **Benson AB**, Venook AP, Al-Hawary MM, Cederquist L, Chen YJ, Ciombor KK, Cohen S, Cooper HS, Deming D, Engstrom PF, Grem JL, Grothey A, Hochster HS, Hoffe S, Hunt S, Kamel A, Kirilcuk N, Krishnamurthi S, Messersmith WA, Meyerhardt J, Mulcahy MF, Murphy JD, Nurkin S, Saltz L, Sharma S, Shibata D, Skibber JM, Sofocleous CT, Stoffel EM, Stotsky-Himelfarb E, Willett CG, Wuthrick E, Gregory KM, Gurski L, Freedman-Cass DA. Rectal Cancer, Version 2.2018, NCCN Clinical Practice Guidelines in Oncology. *J Natl Compr Canc Netw* 2018; **16**: 874-901 [PMID: 30006429 DOI: 10.6004/jnccn.2018.0061]
7 **Sebag-Montefiore D**, Stephens RJ, Steele R, Monson J, Grieve R, Khanna S, Quirke P, Couture J, de Metz C, Myint AS, Bessell E, Griffiths G, Thompson LC, Parmar M. Preoperative radiotherapy versus selective postoperative chemoradiotherapy in patients with rectal cancer (MRC CR07 and NCIC-CTG C016): a multicentre, randomised trial. *Lancet* 2009; **373**: 811-820 [PMID: 19269519 DOI: 10.1016/S0140-6736(09)60484-0]
8 **van Gijn W**, Marijnen CA, Nagtegaal ID, Kranenbarg EM, Putter H, Wiggers T, Rutten HJ, Påhlman L, Glimelius B, van de Velde CJ; Dutch Colorectal Cancer Group. Preoperative radiotherapy combined with total mesorectal excision for resectable rectal cancer: 12-year follow-up of the multicentre, randomised controlled TME trial. *Lancet Oncol* 2011; **12**: 575-582 [PMID: 21596621 DOI: 10.1016/S1470-2045(11)70097-3]
9 **Zhang XM**, Zhang HL, Yu D, Dai Y, Bi D, Prince MR, Li C. 3-T MRI of rectal carcinoma: preoperative diagnosis, staging, and planning of sphincter-sparing surgery. *AJR Am J Roentgenol* 2008; **190**: 1271-1278 [PMID: 18430843 DOI: 10.2214/AJR.07.2505]
10 **Kim H**, Lim JS, Choi JY, Park J, Chung YE, Kim MJ, Choi E, Kim NK, Kim KW. Rectal cancer: comparison of accuracy of local-regional staging with two- and three-dimensional preoperative 3-T MR imaging. *Radiology* 2010; **254**: 485-492 [PMID: 20093520 DOI: 10.1148/radiol.09090587]
11 **Heo SH**, Kim JW, Shin SS, Jeong YY, Kang HK. Multimodal imaging evaluation in staging of rectal cancer. *World J Gastroenterol* 2014; **20**: 4244-4255 [PMID: 24764662 DOI: 10.3748/wjg.v20.i15.4244]
12 **Brouwer NPM**, Stijns RCH, Lemmens VEPP, Nagtegaal ID, Beets-Tan RGH, Fütterer JJ, Tanis PJ, Verhoeven RHA, de Wilt JHW. Clinical lymph node staging in colorectal cancer; a flip of the coin? *Eur J Surg Oncol* 2018; **44**: 1241-1246 [PMID: 29739638 DOI: 10.1016/j.ejso.2018.04.008]
13 **Beets-Tan RGH**, Lambregts DMJ, Maas M, Bipat S, Barbaro B, Curvo-Semedo L, Fenlon HM, Gollub MJ, Gourtsoyianni S, Halligan S, Hoeffel C, Kim SH, Laghi A, Maier A, Rafaelsen SR, Stoker J, Taylor SA, Torkzad MR, Blomqvist L. Magnetic resonance imaging for clinical management of rectal cancer: Updated recommendations from the 2016 European Society of Gastrointestinal and Abdominal Radiology (ESGAR) consensus meeting. *Eur Radiol* 2018; **28**: 1465-1475 [PMID: 29043428 DOI: 10.1007/s00330-017-5026-2]
14 **Padhani AR**, Liu G, Koh DM, Chenevert TL, Thoeny HC, Takahara T, Dzik-Jurasz A, Ross BD, Van Cauteren M, Collins D, Hammoud DA, Rustin GJ, Taouli B, Choyke PL. Diffusion-weighted magnetic resonance imaging as a cancer biomarker: consensus and recommendations. *Neoplasia* 2009; **11**: 102-125 [PMID: 19186405 DOI: 10.1593/neo.81328]
15 **Bassaneze T**, Gonçalves JE, Faria JF, Palma RT, Waisberg J. Quantitative Aspects of Diffusion-weighted Magnetic Resonance Imaging in Rectal Cancer Response to Neoadjuvant Therapy. *Radiol Oncol* 2017; **51**: 270-276 [PMID: 28959163 DOI: 10.1515/raon-2017-0025]
16 **Iannicelli E**, Di Pietropaolo M, Pilozzi E, Osti MF, Valentino M, Masoni L, Ferri M. Value of diffusion-weighted MRI and apparent diffusion coefficient measurements for predicting the response of locally advanced rectal cancer to neoadjuvant chemoradiotherapy. *Abdom Radiol (NY)* 2016; **41**: 1906-1917 [PMID: 27323759 DOI: 10.1007/s00261-016-0805-9]

17 **Just N**. Improving tumour heterogeneity MRI assessment with histograms. *Br J Cancer* 2014; **111**: 2205-2213 [PMID: 25268373 DOI: 10.1038/bjc.2014.512]
18 **Aker M**, Ganeshan B, Afaq A, Wan S, Groves AM, Arulampalam T. Magnetic Resonance Texture Analysis in Identifying Complete Pathological Response to Neoadjuvant Treatment in Locally Advanced Rectal Cancer. *Dis Colon Rectum* 2019; **62**: 163-170 [PMID: 30451764 DOI: 10.1097/DCR.0000000000001224]
19 **Xia KJ**, Yin HS, Qian PJ, Jiang YZ. Liver Semantic Segmentation Algorithm Based on Improved Deep Adversarial Networks in combination of Weighted Loss Function on Abdominal CT Images. *IEEE Access* 2019; **7**: 96349-96358 [DOI: 10.1109/ACCESS.2019.2929270]
20 **Ytre-Hauge S**, Dybvik JA, Lundervold A, Salvesen ØO, Krakstad C, Fasmer KE, Werner HM, Ganeshan B, Høivik E, Bjørge L, Trovik J, Haldorsen IS. Preoperative tumor texture analysis on MRI predicts high-risk disease and reduced survival in endometrial cancer. *J Magn Reson Imaging* 2018; **48**: 1637-1647 [PMID: 30102441 DOI: 10.1002/jmri.26184]
21 **Ueno Y**, Forghani B, Forghani R, Dohan A, Zeng XZ, Chamming's F, Arseneau J, Fu L, Gilbert L, Gallix B, Reinhold C. Endometrial Carcinoma: MR Imaging-based Texture Model for Preoperative Risk Stratification-A Preliminary Analysis. *Radiology* 2017; **284**: 748-757 [PMID: 28493790 DOI: 10.1148/radiol.2017161950]
22 **Becker AS**, Ghafoor S, Marcon M, Perucho JA, Wurnig MC, Wagner MW, Khong PL, Lee EY, Boss A. MRI texture features may predict differentiation and nodal stage of cervical cancer: a pilot study. *Acta Radiol Open* 2017; **6**: 2058460117729574 [PMID: 29085671 DOI: 10.1177/2058460117729574]
23 **Ahmed A**, Gibbs P, Pickles M, Turnbull L. Texture analysis in assessment and prediction of chemotherapy response in breast cancer. *J Magn Reson Imaging* 2013; **38**: 89-101 [PMID: 23238914 DOI: 10.1002/jmri.23971]
24 **Ng F**, Ganeshan B, Kozarski R, Miles KA, Goh V. Assessment of primary colorectal cancer heterogeneity by using whole-tumor texture analysis: contrast-enhanced CT texture as a biomarker of 5-year survival. *Radiology* 2013; **266**: 177-184 [PMID: 23151829 DOI: 10.1148/radiol.12120254]
25 **Ganeshan B**, Skogen K, Pressney I, Coutroubis D, Miles K. Tumour heterogeneity in oesophageal cancer assessed by CT texture analysis: preliminary evidence of an association with tumour metabolism, stage, and survival. *Clin Radiol* 2012; **67**: 157-164 [PMID: 21943720 DOI: 10.1016/j.crad.2011.08.012]
26 **Field A**. Discovering Statistics Using IBM SPSS Statistics. 4th ed. New Delhi: Sage Publications Ltd, 2013
27 **Gollub MJ**, Lakhman Y, McGinty K, Weiser MR, Sohn M, Zheng J, Shia J. Does gadolinium-based contrast material improve diagnostic accuracy of local invasion in rectal cancer MRI? A multireader study. *AJR Am J Roentgenol* 2015; **204**: W160-W167 [PMID: 25615776 DOI: 10.2214/AJR.14.12599]
28 **Al-Sukhni E**, Milot L, Fruitman M, Beyene J, Victor JC, Schmocker S, Brown G, McLeod R, Kennedy E. Diagnostic accuracy of MRI for assessment of T category, lymph node metastases, and circumferential resection margin involvement in patients with rectal cancer: a systematic review and meta-analysis. *Ann Surg Oncol* 2012; **19**: 2212-2223 [PMID: 22271205 DOI: 10.1245/s10434-011-2210-5]
29 **Kierans AS**, Rusinek H, Lee A, Shaikh MB, Triolo M, Huang WC, Chandarana H. Textural differences in apparent diffusion coefficient between low- and high-stage clear cell renal cell carcinoma. *AJR Am J Roentgenol* 2014; **203**: W637-W644 [PMID: 25415729 DOI: 10.2214/AJR.14.12570]
30 **Mu W**, Chen Z, Liang Y, Shen W, Yang F, Dai R, Wu N, Tian J. Staging of cervical cancer based on tumor heterogeneity characterized by texture features on (18)F-FDG PET images. *Phys Med Biol* 2015; **60**: 5123-5139 [PMID: 26083460 DOI: 10.1088/0031-9155/60/13/5123]
31 **Liu L**, Liu Y, Xu L, Li Z, Lv H, Dong N, Li W, Yang Z, Wang Z, Jin E. Application of texture analysis based on apparent diffusion coefficient maps in discriminating different stages of rectal cancer. *J Magn Reson Imaging* 2017; **45**: 1798-1808 [PMID: 27654307 DOI: 10.1002/jmri.25460]
32 **Attenberger UI**, Pilz LR, Morelli JN, Hausmann D, Doyon F, Hofheinz R, Kienle P, Post S, Michaely HJ, Schoenberg SO, Dinter DJ. Multi-parametric MRI of rectal cancer - do quantitative functional MR measurements correlate with radiologic and pathologic tumor stages? *Eur J Radiol* 2014; **83**: 1036-1043 [PMID: 24791649 DOI: 10.1016/j.ejrad.2014.03.012]
33 **Vignati A**, Mazzetti S, Giannini V, Russo F, Bollito E, Porpiglia F, Stasi M, Regge D. Texture features on T2-weighted magnetic resonance imaging: new potential biomarkers for prostate cancer aggressiveness. *Phys Med Biol* 2015; **60**: 2685-2701 [PMID: 25768265 DOI: 10.1088/0031-9155/60/7/2685]
34 **Li W**, Jiang Z, Guan Y, Chen Y, Huang X, Liu S, He J, Zhou Z, Ge Y. Whole-lesion Apparent Diffusion Coefficient First- and Second-Order Texture Features for the Characterization of Rectal Cancer Pathological Factors. *J Comput Assist Tomogr* 2018; **42**: 642-647 [PMID: 29613992 DOI: 10.1097/RCT.0000000000000731]
35 **Huang YQ**, Liang CH, He L, Tian J, Liang CS, Chen X, Ma ZL, Liu ZY. Development and Validation of a Radiomics Nomogram for Preoperative Prediction of Lymph Node Metastasis in Colorectal Cancer. *J Clin Oncol* 2016; **34**: 2157-2164 [PMID: 27138577 DOI: 10.1200/JCO.2015.65.9128]
36 **Lubner MG**, Smith AD, Sandrasegaran K, Sahani DV, Pickhardt PJ. CT Texture Analysis: Definitions, Applications, Biologic Correlates, and Challenges. *Radiographics* 2017; **37**: 1483-1503 [PMID: 28898189 DOI: 10.1148/rg.2017170056]
37 **Monson JR**, Weiser MR, Buie WD, Chang GJ, Rafferty JF, Buie WD, Rafferty J; Standards Practice Task Force of the American Society of Colon and Rectal Surgeons. Practice parameters for the management of rectal cancer (revised). *Dis Colon Rectum* 2013; **56**: 535-550 [PMID: 23575392 DOI: 10.1097/DCR.0b013e31828cb66c]

Published By Baishideng Publishing Group Inc
7041 Koll Center Parkway, Suite 160, Pleasanton, CA 94566, USA
Telephone: +1-925-3991568
E-mail: bpgoffice@wjgnet.com
Help Desk:http://www.f6publishing.com/helpdesk
http://www.wjgnet.com